Fluid Phase Behavior from Molecular Simulation: Hydrazine, Monomethylhydrazine, Dimethylhydrazine and Binary Mixtures Containing These Compounds

Ekaterina Elts[1], Thorsten Windmann[1], Daniel Staak[2], Jadran Vrabec[1] *

[1] Lehrstuhl für Thermodynamik und Energietechnik, Universität Paderborn, Warburger Straße 100, 33098 Paderborn, Germany

[2] Lonza AG, Chemical Research and Development, CH-3930 Visp, Switzerland

Keywords: Molecular modeling and simulation; vapor-liquid equilibrium; Henry's law constant; Hydrazine; Monomethylhydrazine; Dimethylhydrazine; Argon; Nitrogen; Carbon Monoxide; Ammonia; Water

Abstract

New molecular models for Hydrazine and its two most important methylized derivatives (Monomethylhydrazine and Dimethylhydrazine) are proposed to study the fluid phase behavior of these hazardous compounds. A parameterization of the classical molecular interaction models is carried out by using quantum chemical calculations and subsequent fitting to experimental vapor pressure and saturated liquid density data. To validate the molecular models, vapor-liquid equilibria for the pure hydrazines and binary hydrazine mixtures with Water and Ammonia are calculated and compared with the available experimental data. In addition, the Henry's law constant for the physical solubility of Argon, Nitrogen and Carbon Monoxide in liquid Hydrazine, Monomethylhydrazine and Dimethylhydrazine is computed. In general, the simulation results are in very good agreement with the experimental data.

---

* corresponding author, tel.: +49-5251/60-2421, fax: +49-5251/60-3522, email: jadran.vrabec@upb.de

1 Introduction

On October 24, 1960, the greatest disaster in the history of rocketry, now also known as Nedelin disaster, occurred [1–3]. At that time, the Soviet newspapers published only a short communique informing that Marshall of Artillery Mitrofan Nedelin has died in an airplane crash. No details about the accident or the names of other victims have been released. It took almost three decades before the first publication in the official Soviet press shed light on what really had happened at Baikonur Cosmodrome during the development of the Soviet R-16 intercontinental ballistic missile (ICBM) under the direction of Marshall Nedelin, the commander of the Soviet Strategic Rocket Forces.

The R-16 ICBM was considered a top priority by the Soviet leadership, being the first Soviet rocket designed to use a fuel composed of a Hydrazine derivative, i.e. unsymmetrical 1,1-Dimethylhydrazine. This fluid is extremely toxic, but is at the same time a very reactive and efficient reagent, which in combination with Dinitrogen Tetroxide as fuel oxidant gave the missile a much faster response time than all other propellants used before [1,2].

In October 1960, the design team worked furiously to complete the first R-16 rocket as soon as possible and hoped to produce a successful launch before the November 7 anniversary of the Bolshevik Revolution [3]. Due to the time pressure, some important technical problems, like leaks after the fueling of the rocket and electrical faults preventing the proper work of the propellant pumps, were underestimated and neglected. Moreover, the safety rules were ignored, and numerous people, which were supposed to leave the launch area, stayed at the pad [1–3].

Around 30 minutes before the scheduled launch, when an estimated 250 personnel and visitors, including Marshal Nedelin and several constructors, were still around the rocket, the second stage engine ignited. Instantly, the roaring flame of the engine burst through the fuel tank of the first stage directly below, creating a massive explosion that sprayed acidic chemicals across the launch complex. In seconds, a giant fireball, up to 120 meters in diameter, engulfed the area. Massive explosions continued to rock the launch pad for about 20 seconds, and the subsequent fires lasted for two hours. The blast was reportedly visible as far as 50 km away [2]. People near the rocket were instantly incinerated, those further away were burned to death or poisoned by the resulting toxic gases. The official death toll was 92 [1], however, the true casualty

list has remained a mystery. The best estimate appears to be around 122 fatalities. This number includes 74 killed in the blast and 48 who died over subsequent weeks from injuries due to burns or exposure to toxic chemicals [2].

This tragical story is one of many illustrations, how dangerous Hydrazine and its derivatives are. It is also well known that the carcinogenic and toxicologic consequences associated with inhalation or ingestion of Hydrazine include damage to internal organs, creation of blood abnormalities, irreversible deterioration of the nervous system, and even teratogenic and mutagenic effects [4].

On the other hand, these multi-purpose chemical reagents have a variety of applications. Along with their use as high-energy propellants in thrusters for rockets, satellites and space shuttles, they also have a number of commercial applications, including their role as essential building blocks in the synthesis of various polymers, pesticides, pharmaceuticals and chemotherapeutic agents. Furthermore, they are used as explosives to military fuel cells, in metal finishing (nickel plating), in boiler water-feed deoxygenation, in photographic development etc. [4–7].

Due to the safety issues associated with the handling of Hydrazine and its derivatives, molecular modeling and simulation can play a particularly important role for the investigation of the thermodynamic properties of these fluids. This approach is based on the numerical description of the molecular interactions and allows to determine any thermodynamic property in a consistent manner.

However, classical molecular simulations, comprising molecular dynamics (MD) and Monte Carlo (MC) calculations, are still uncommon for Hydrazine and its derivatives in the scientific literature, especially for the description of vapor-liquid equilibria of these fluids. On the other hand, a few force field parameters and models have been recently published for these chemicals [5,8]. The force field developed by Borodin [8] accurately describes the thermodynamic and transport properties of Hydrazine and its derivatives in one liquid state. Unfortunately, no validation against vapor-liquid equilibrium (VLE) data has been done, being much more difficult. A force field recently developed by Gutowski et al. [5] was validated against experimental saturated densities, vapor pressure, heat of vaporization, isobaric heat capacity and self-diffusion coefficient. While it yields satisfactory results for the liquid density and the heat of vaporization, the vapor pressure predicted for Hydrazine and its derivatives deviates significantly from experimental

data.

This work presents new molecular models for Hydrazine (N_2H_4), Monomethylhydrazine (CH_3-NH-NH_2) and 1,1-Dimethylhydrazine ((CH_3)$_2$-N-NH_2). The parameterization of the molecular interaction models for these pure substances was carried out on the basis of the quantum chemical (QC) calculations, followed by optimizations to the experimental vapor pressure and saturated liquid density. The molecular interaction models were then used to predict important thermodynamic properties and to study the fluid phase behavior. Thereby, a large set of experimental thermodynamic data for pure hydrazines and binary hydrazine mixtures was considered for comparison with the present molecular simulation data. Binary hydrazine mixtures with the following components were simulated: Argon (Ar), Nitrogen (N_2), Carbon Monoxide (CO), Ammonia (NH_3) and Water (H_2O).

2 Molecular model class

The present molecular models include three groups of parameters. These are (1) the geometric parameters, specifying the positions of different interaction sites, (2) the electrostatic parameters, defining the polar interactions in terms of point charges, dipoles or quadrupoles, and (3) the dispersive and repulsive parameters, determining the attraction by London forces and the repulsion by electronic orbital overlaps. Here, the Lennard-Jones (LJ) 12-6 potential [9,10] was used to describe the dispersive and repulsive interactions. The total intermolecular interaction energy thus writes as

$$
U = \sum_{i=1}^{N-1} \sum_{j=i+1}^{N} \left\{ \sum_{a=1}^{S_i^{\mathrm{LJ}}} \sum_{b=1}^{S_j^{\mathrm{LJ}}} 4\varepsilon_{ijab} \left[\left(\frac{\sigma_{ijab}}{r_{ijab}} \right)^{12} - \left(\frac{\sigma_{ijab}}{r_{ijab}} \right)^{6} \right] + \right.
$$
$$
\sum_{c=1}^{S_i^{\mathrm{e}}} \sum_{d=1}^{S_j^{\mathrm{e}}} \frac{1}{4\pi\epsilon_0} \left[\frac{q_{ic}q_{jd}}{r_{ijcd}} + \frac{q_{ic}\mu_{jd} + \mu_{ic}q_{jd}}{r_{ijcd}^2} \cdot f_1(\boldsymbol{\omega}_i, \boldsymbol{\omega}_j) + \frac{q_{ic}Q_{jd} + Q_{ic}q_{jd}}{r_{ijcd}^3} \cdot f_2(\boldsymbol{\omega}_i, \boldsymbol{\omega}_j) + \right.
$$
$$
\left. \left. \frac{\mu_{ic}\mu_{jd}}{r_{ijcd}^3} \cdot f_3(\boldsymbol{\omega}_i, \boldsymbol{\omega}_j) + \frac{\mu_{ic}Q_{jd} + Q_{ic}\mu_{jd}}{r_{ijcd}^4} \cdot f_4(\boldsymbol{\omega}_i, \boldsymbol{\omega}_j) + \frac{Q_{ic}Q_{jd}}{r_{ijcd}^5} \cdot f_5(\boldsymbol{\omega}_i, \boldsymbol{\omega}_j) \right] \right\}, \quad (1)
$$

where r_{ijab}, ε_{ijab}, σ_{ijab} are the distance, the LJ energy parameter and the LJ size parameter, respectively, for the pair-wise interaction between LJ site a on molecule i and LJ site b on molecule j. The permittivity of the vacuum is ϵ_0, whereas q_{ic}, μ_{ic} and Q_{ic} denote the point charge magnitude, the dipole moment and the quadrupole moment of the electrostatic interaction site c on molecule i and so forth. The expressions

$f_x(\boldsymbol{\omega}_i, \boldsymbol{\omega}_j)$ stand for the dependency of the electrostatic interactions on the orientations $\boldsymbol{\omega}_i$ and $\boldsymbol{\omega}_j$ of the molecules i and j, cf. [11,12]. Finally, the summation limits N, S_x^{LJ} and S_x^{e} denote the number of molecules, the number of LJ sites and the number of electrostatic sites, respectively.

It should be noted that a point dipole may, e.g. when a simulation program does not support this interaction site type, be approximated by two point charges $\pm q$ separated by a distance l. Limited to small l, this distance may be chosen freely as long as $\mu = ql$ holds. Analogously, a linear point quadrupole can be approximated by three collinear point charges q, $-2q$, and q separated by l each, where $Q = 2ql^2$ [13].

For a given molecule, i.e. for a pure fluid throughout, the interactions between LJ sites of different type were defined here by applying the standard Lorentz-Berthelot combining rules [14,15]

$$\sigma_{ijab} = \frac{\sigma_{iiaa} + \sigma_{jjbb}}{2}, \tag{2}$$

and

$$\varepsilon_{ijab} = \sqrt{\varepsilon_{iiaa}\varepsilon_{jjbb}}. \tag{3}$$

3 Molecular pure substance models

All molecules studied in the present work do not exhibit significant conformational changes. Hence their internal degrees of freedom were neglected and the molecular models were chosen to be rigid. As a first step, the geometric data of the molecules, i.e. bond lengths, angles and dihedrals, were determined by QC calculations. Therefore, a geometry optimization was performed via an energy minimization using the GAMESS (US) package [16]. The Hartree-Fock level of theory was applied with a relatively small (6-31G) basis set.

3.1 Hydrazine

The present Hydrazine (N_2H_4) model consists of two LJ sites, located exactly at the positions of the Nitrogen atoms, plus six point charges, i.e. one for every atom. All LJ parameters and the charge magnitudes were initially taken from the Monomethylamine model of Schnabel et al. [17].

During the model parameter optimization to vapor pressure and saturated liquid density, the distance

between two atoms of Nitrogen as determined by QC (1.414 Å) was slightly reduced, leading to a distance of 1.4 Å and the point charge magnitudes were adjusted. Finally, the reduced unit method [18] for fine-tuning the model parameters to the experimental VLE data was used, leading to a slight modification of all model parameter values. The full parameter set of the new Hydrazine model is listed in Table 1.

It should be noted that the final geometrical and electrostatic model parameter values correspond well with the results recently presented by Kaczmarek et al. [19]. In Ref. [19], structural and electronic properties of the Hydrazine molecule were studied by a series of classical and quantum ab initio simulations at room temperature. Therefore, time-average statistical analyses of ab initio MD and ab initio path integral MD simulations of hydrazine were carried out [19]. The values of the normalized distribution functions, corresponding to the present optimized structural molecular model parameters, lie close to the respective normal distribution maximum. The dipole moment magnitude calculated for the present molecular model is about 2.25 D and agrees well with the static equilibrium value of about 2.22 D by Kaczmarek et al. [19]. However, both dipole moments are above the experimental value of 1.85 D reported by Seddon et al. [20].

The results for saturated densities, vapor pressure and heat of vaporization obtained with the present model are compared to the available experimental data [5,21,22] and to the simulation results by Gutowski et al. [5] in Figures 1 to 5. The present data are given in numerical form in the supplementary material. While the model by Gutowski et al. [5] covers the saturated liquid density well only at lower temperatures, deviating from experimental data from by +0.2% at 298 K to -5.1% at 450 K [5], the present model is excellent in the whole temperature range for this property, yielding a mean unsigned error of about 0.5 %, cf. Figure 1. Gutowski et al. [5] overestimated the vapor pressure by more than 130 % at 450 K, while the average deviation for the present model is about 7.6%, cf. Figures 2 and 3. Gutowski et al. [5] did not calculate VLE data above 450 K, but it can be seen from the temperature trend that the deviations would increase there. Both models were also validated against the enthalpy of vaporization. The model by Gutowski et al. [5] exhibits a minimum difference between experiment and simulation of 1.6 kJ/mol at 298.15 K, which is about 3.5 %, however, the deviations again increase significantly with increasing temperature, cf. Figure 4. The results obtained with the present model overestimate the available experimental data on average by about 2.3%.

The critical values of temperature, density and pressure were calculated from the present simulation data with a method suggested by Lotfi et al. [23]. The obtained values are listed in Table 2. The simulated critical data for temperature and pressure of 647.6 K and 13.04 MPa are in good agreement with the experimental values of 653.00 K and 14.69 MPa from the DDB data base [21] and with the experimental values of 653.15 K and 14.69 MPa from the DIPPR [22] and MDB data bases [24]. The critical density from the present simulations is 10.16 mol/l, while the experimental value for this property is about 6.33 mol/l according to the DIPPR and MDB data bases, 7.18 mol/l according to experimental data by Haws and Harden [25] and 10.41 mol/l according to the DDB data base. It should be noted that the critical constants of Hydrazine are very difficult to determine experimentally, because of the tendency of Hydrazine to undergo decomposition at higher temperatures [6,26]. By visual inspection of Figure 1 it can be inferred that the critical density reported in the DIPPR and MDB data bases as well as the experimental critical value by Haws and Harden [25] does not correspond well with the experimental data on the saturated liquid line. Gutowski et al. [5] predicted a critical temperature and density of 593 K and 10.61 mol/l.

Figure 5 presents the isobaric heat capacity of Hydrazine in the homogeneous liquid at ambient pressure. Note that only the residual isobaric heat capacity $c_p^r(T, p)$ was calculated here by molecular simulation. To obtain the total isobaric heat capacity c_p, the solely temperature dependent ideal gas contribution $c_p^\circ(T)$ from the DIPPR data base [22] was added $c_p(T, p) = c_p^\circ(T) + c_p^r(T, p)$. The isobaric heat capacity from the model by Gutowski et al. [5] is in reasonable agreement with the experiment (10.3% deviation), while the difference between experiment and simulation is about 17% for the present model.

Figure 6 compares the simulation results with experimental data on the density of liquid Hydrazine at 0.1013 MPa. The achieved agreement over a temperature range of about 150 K is excellent, yielding a mean unsigned error of only about 0.05%.

For Hydrazine, data on the second virial coefficient from the DIPPR data base [22] are available for comparison with the simulation results. There are two different datasets: approximate values by Drago and Sisler [27] and values estimated with the method by Tsonopoulos [22,28]. The DIPPR correlation is based on the estimated values, cf. Figure 7. The present simulation results agree well with the estimated data [22,28], only at low temperatures some noticeable deviations are present, yielding a mean error of

about 0.11 l/mol. The approximate second virial coefficient data between 363 and 393 K by Drago and Sisler [27] are between +2.14 and +4.20 l/mol (far out of scale in Figure 7) and seem to be wrong.

Figure 8 compares the predictions based on the present molecular model with the experimental data on the shear viscosity available in DDB data base [21]. The results obtained with the present model overestimate the experimental shear viscosity data by about 64 %.

3.2   Monomethylhydrazine

The intermolecular interactions of Monomethylhydrazine (CH_3-NH-NH_2) were described by three LJ sites, i.e. one for every atomic group. In addition, three point charges were located exactly at the positions of the Hydrogen atoms and the Nitrogen atom of the NH_2 group. The LJ parameters of the NH_2 and NH groups and the charge magnitudes of the NH_2 group were taken from the present Hydrazine model. The LJ parameters of the CH_3 group were taken from the Ethanol (and Monomethylamine) model by Schnabel et al. [17,29].

During the model parameter optimization to vapor pressure and saturated liquid density, the distance between the CH_3 group and the NH group was increased, leading to a distance of 1.7 Å which is larger than the one determined by QC (1.458 Å) and the experimental value of 1.47 Å from Schmidt [6]. The full parameter set of the molecular Monomethylhydrazine model is listed in Table 1.

The results for saturated densities, vapor pressure and heat of vaporization are compared to the available experimental data [5,21,22] and to the simulation results by Gutowski et al. [5] in Figures 1 to 5. The present data are given in numerical form in the supplementary material. The present model describes the vapor pressure and the saturated densities much better than the model by Gutowski et al. [5], which underestimates the experimental saturated liquid density from 2.8 % at 273 K to 7.7 % at 450 K [5]. These deviations are minor for the present model, yielding a mean unsigned error of about 0.2 % over the entire temperature range, cf. Figure 1. The vapor pressure by Gutowski et al. [5] is on average by 54% below the experimental data, while the average deviation for the present model is about 7.0 %, cf. Figures 2 and 3. The enthalpy of vaporization deviates from the experimental data for both molecular models, cf. Figure 4. The simulation results by Gutowski et al. [5] are higher than the experimental data by about 6.7 % and

also show a significant scatter, cf. Figure 4. The results obtained with the present model underestimate the available experimental enthalpy of vaporization data by about 5.1 %.

The critical values of temperature, density and pressure predicted with the present model using the method by Lotfi et al. [23] are given in Table 2. The critical temperature of 606.6 K is by almost 22 K higher than the experimental value by Schmidt [6] and by almost 40 K than the experimental value from the DDB and MDB data bases [21,24]. The present critical density is 6.53 mol/l, while the experimental value for this property is only about 3.69 mol/l according to the DDB and MDB data bases and 6.29 mol/l according to experimental data by Schmidt [6]. The present critical pressure of 7.66 MPa is in good agreement with the experimental values of 8.04 MPa, 8.24 MPa and 8.21 from the DDB and MDB data bases and by Schmidt [6], respectively. In this case, the critical temperature of 595 K and the critical density of 6.07 mol/l predicted by Gutowski et al. [5] are slightly closer to the experimental data.

The isobaric heat capacity of the homogeneous liquid at ambient pressure from simulation is in reasonable agreement with the experimental data for both models. The average deviation is 9.7 % for the model by Gutowski et al. [5] and -8.8 % for the present model, cf. Figure 5.

Figure 7 shows the second virial coefficient predicted with the present model. Unfortunately, no other data are available for comparison.

3.3   Dimethylhydrazine

The present molecular model for 1,1-Dimethylhydrazine ($(CH_3)_2$-N-NH_2) is based on the Hydrazine and Monomethylhydrazine models described above. This model consists of four LJ sites, i.e. one for every atomic group, plus three point charges, located exactly at the positions of the Hydrogen atoms and the Nitrogen atom of the NH_2 group, like in case of the Monomethylhydrazine model. The LJ parameters and the charge magnitudes for the NH_2 group were taken from the Hydrazine model. The LJ parameters for the Nitrogen atom were taken from a Nitrogen model developed earlier [30], the LJ parameters for the CH_3 group were taken from the Ethanol (and Monomethylamine) model by Schnabel et al. [17,29].

In case of the Dimethylhydrazine model, only the geometry parameters, initially determined by QC, were optimized to the experimental homogeneous liquid density. For this, the distances between the Nitrogen

atom and the CH$_3$ groups were adjusted, leading to a distance of 1.59 Å, which is somewhat larger than the distance determined by QC (1.46 Å) and than the experimental value of 1.47 ± 0.03 Å by Beamer [6,31]. The full parameter set of the new molecular Dimethylhydrazine model is listed in Table 1.

The results for saturated densities, vapor pressure and heat of vaporization are compared to the available experimental data [5,21,22] and to the simulation results by Gutowski et al. [5] in Figures 1 to 5. The present data are given in numerical form in the supplementary material. The saturated liquid density based on the model by Gutowski et al. [5] follows an opposite trend relative to Hydrazine and Monometylhydrazine, i.e. the density from simulation is larger than from experiment [5]. Over the temperature range from 273 to 339 K, the values by Gutowski are in excellent agreement with the experiment, being only slightly higher (0.5 to 1.7 %) [5]. At higher temperatures the deviations are increasing. For the present model, the average deviation from the experimental saturated liquid density is about 1.3 % over the whole temperature range. In case of the vapor pressure, the present model yields very good results, deviating from the experiment only by about 3.7 %, while the values by Gutowski et al. [5] underestimate the experimental vapor pressure by more than 80 % above 340 K.

The critical properties were determined through fits to the present VLE simulation results as suggested by Lotfi et al. [23]. Table 2 compares these properties to the experimental data from Schmidt [6]. The present critical data for temperature and density of 514.46 K and 4.95 mol/l are in good agreement with the experimental values of 523 K and 4.58 mol/l, while Gutowski et al. [5] predicted a critical temperature of 616 K, which is too high by more than 90 K, and a critical density of 4.49 mol/l. The present critical pressure of 5.0 MPa is in very good agreement with the experimental value of 5.4 MPa reported by Schmidt [6].

The enthalpy of vaporization presented by Gutowski et al. [5] at 298 and 339 K is higher than the experimental values by around 8 kJ/mol, which is 24% in relative terms. For the present model, these deviations are minor, yielding a mean unsigned error of about 1.0 %, cf. Figure 4. It should be noted that Gutowski et al. [5] predicted enthalpy of vaporization data which is only little dependent on the type of hydrazine, cf. Figure 4. This finding is contradictory to the available experimental data. On the other hand, the homogeneous liquid isobaric heat capacity of Dimethylhydrazine by Gutowski et al. [5] is in excellent agreement

with the experiment [32], differing by only 0.4 %, while the deviation for the present model is about 5.9 %, cf. Figure 5.

Figure 6 compares the present simulation results with experimental data on the density of homogeneous liquid Dimethylhydrazine at ambient pressure. The achieved agreement is good, yielding a mean unsigned error of about 1.1%.

Figure 7 shows the second virial coefficient predicted with the present model. Unfortunately, no other data are available for comparison.

3.4 Other molecular models

The present work is devoted to the development and assessment of molecular models for Hydrazine and its two most important methylized derivatives. Apart from VLE and homogeneous liquid data for the pure hydrazines, the majority of the publicly available experimental data for binary mixtures containing hydrazines were used to validate the new molecular models. Binary hydrazine mixtures with the following components were simulated: Argon (Ar), Nitrogen (N_2), Carbon Monoxide (CO), Ammonia (NH_3) and Water (H_2O). The molecular models used in this work for these compounds are briefly described in the following.

Molecular models for Argon, Nitrogen and Carbon Monoxide, used here to calculate the Henry's law constant in liquid Hydrazine, Monomethylhydrazine and Dimethylhydrazine, were taken from Vrabec et al. [30] (Ar and N_2) and Stoll et al. [33] (CO). These are a spherical non-polar one-center Lennard-Jones (LJ) model for Ar, an elongated dipolar two-center Lennard-Jones (2CLJD) model for CO and an elongated quadrupolar two-center Lennard-Jones (2CLJQ) model for N_2. These models describe the VLE with an accuracy of about 0.5 % for the saturated liquid density, 3-4 % for the vapor pressure and 2-3 % for the enthalpy of vaporization over the whole temperature range from the triple point to the critical point [30,33].

The molecular model for Ammonia, used here to calculate VLE of binary mixtures with all three studied hydrazines, was taken from Eckl et al. [34]. It consists of a single Lennard-Jones site for the dispersive and repulsive interactions. The electrostatic interactions as well as hydrogen bonding were modeled by a total

11

of four superimposed partial charges. The model by Eckl et al. [34] shows mean unsigned deviations to experimental data of 0.7 % for the saturated liquid density, 1.6 % for the vapor pressure and 2.7 % for the enthalpy of vaporization over the whole temperature range from the triple point to the critical point [34].

The employed Water model is based on the rigid four-site TIP4P model type, initially proposed by Jorgensen et al. [35]. This model type consists of three point charges, eccentrically superimposed to a single LJ site. The TIP4P model type was parametrized by many authors [36]. Here, the interaction parameters by Huang et al. [37,38] were used. In comparison with alternative parametrizations from the literature [35,39–42], this model better represents the VLE properties, if the whole temperature range is considered. The model by Huang et al. [37,38] yields mean unsigned errors for vapor pressure, saturated liquid density and enthalpy of vaporization of 7.2, 1.1 and 2.8 %, respectively, in the temperature range from 300 to 600 K, which is about 46 to 93 % of the critical temperature [38].

4 Molecular mixture models

On the basis of defined pairwise additive pure fluid models, molecular modeling of mixtures reduces to modeling the interactions between unlike molecules. Unlike interactions consist of two different types here. The unlike electrostatic interactions, e.g. between charges, dipoles or quadrupoles, were treated in a physically straightforward way, simply using the laws of electrostatics.

Unfortunately, the unlike dispersive attraction is not straightforward. If a mixture A + B is modeled on the basis of Lennard-Jones potentials, the knowledge of the unlike LJ parameters σ_{ijab} and ε_{ijab} for the pairwise interaction between LJ site a on molecule i of component A and LJ site b on molecule j of component B is required. Due to the fact that there is no sound physical framework for their determination, the broadly used Lorentz-Berthelot combining rules are the usual starting point [43]. Applying σ_{ijab} and ε_{ijab} as given by equations (2) and (3) allows for the prediction of mixture properties from pure fluid data alone [43–47]. But as shown in these publications, a significant improvement can be achieved by introducing one state independent binary interaction parameter ξ to adjust the unlike energy parameter

$$\varepsilon_{ijab} = \xi \sqrt{\varepsilon_{iiaa}\varepsilon_{jjbb}}. \tag{4}$$

12

It allows to fine-tune the unlike dispersive attraction, a property which is very challenging even for current QC approaches [48]. It should be pointed out that A and B are molecule species that may each be described by several LJ sites with different energy parameters ϵ. Thus, ξ is a single overall parameter that acts consistently on all individual unlike LJ interactions of the pair A + B.

For VLE, it was shown in [43] that ξ can be adjusted to a single experimental binary vapor pressure. Specifying temperature and saturated liquid composition, ξ has hardly any influence on the saturated liquid density and a minor influence on the saturated vapor composition. The benefit of ξ lies in a significantly enhanced representation of the two-phase envelope. The binary interaction parameter was adjusted here following the same procedure as in [44–47,49].

5 Peng-Robinson equation of state

Cubic equations of state (EOS) are excellent tools to correlate experimental data and are therefore a workhorse for many technical applications. In the present work, the Peng-Robinson EOS with the quadratic Van der Waals one-fluid mixing rule was used to adjust binary experimental data. The Peng-Robinson EOS [50] is given by

$$p = \frac{RT}{v - b} - \frac{a}{v(v + b) + b(v - b)}, \tag{5}$$

where the temperature dependent parameter a is defined by

$$a = \left(0.45724 \, \frac{R^2 T_c{}^2}{p_c}\right) \left[1 + \left(0.37464 + 1.54226 \, \omega - 0.26992 \, \omega^2\right) \left(1 - \sqrt{\frac{T}{T_c}}\right)\right]^2. \tag{6}$$

The constant parameter b is

$$b = 0.07780 \, \frac{RT_c}{p_c}. \tag{7}$$

Therein, critical temperature T_c, critical pressure p_c, acentric factor ω and the molar mass M of the pure substance are needed, cf. Table 3. Tabulated values [6,21,22,24–26] were taken for Hydrazine and Monomethylhydrazine. For Dimethylhydrazine, no experimental critical pressure was available to us when this work was carried out so that the present simulation value was used instead. The same holds for the acentric factor ω. The experimental critical pressure of Dimethylhydrazine (5.4 MPa [6]), which we retrieved subsequently, does not differ too much from the present simulation value (5.0 MPa) so that we

did not repeat the EOS calculations with the experimental value.

To apply the Peng-Robinson EOS to mixtures, mixed parameters a_m and b_m have to be defined. For this purpose, a variety of mixing rules can be found in the literature. Here, the quadratic Van der Waals one-fluid mixing rule [50] was chosen. It states that the pure substance parameters a and b have to be replaced by

$$a_m = \sum_i \sum_j x_i x_j a_{ij}. \tag{8}$$

The indices i and j denote the components, with

$$a_{ij} = \sqrt{a_i a_j}(1 - k_{ij}), \tag{9}$$

where k_{ij} is an adjustable binary parameter to correlate experimental data. The constant parameter of the mixture is defined as

$$b_m = \sum_i x_i b_i. \tag{10}$$

This classical thermodynamic model was used to fit the experimental VLE data of all three binary combinations with Ammonia and Water as well as of the mixture Dimethylhydrazine + Hydrazine. The binary parameter k_{ij} was throughout adjusted to the same experimental data as the binary interaction parameter of the molecular models ξ, cf. Table 4. The results of the Peng-Robinson EOS are presented below and validated by comparison to data from experiment and simulation.

6 Binary vapor-liquid equilibria

Based on the discussed three molecular hydrazine models, VLE data were predicted for all three binary combinations with Water as well as for the mixture Dimethylhydrazine + Hydrazine. Also all binary combinations of the three hydrazines with Ammonia at different temperatures were simulated. This choice was driven by the availability of experimental VLE data. Present simulation data for all mixtures are given in numerical form in the supplementary material. Please note that this material also contains the saturated densities and the heat of vaporization for all regarded mixtures. These data are not further discussed here, because of the lack of experimental data for comparison.

For orientation and comparison, the results of the Peng-Robinson EOS [51] with adjusted binary parameter

k_{ij} of the quadratic mixing rule are also presented. Generally, the EOS was optimized to the experimental vapor pressure at the same state point as the molecular mixture model.

6.1 Water + Hydrazine

For most uses, hydrazine is produced as Hydrazine Hydrate in a formulation with Water [6,52]. Hydrazine Hydrate, or simply the aqueous solution of Hydrazine, finds use in water treatment as Oxygen scavenger in high pressure boilers and in the synthesis of various chemicals and bulk drugs. Anhydrous Hydrazine is the formulation used for rocket fuels and is produced by dehydration of the hydrate via azeotropic distillation with e.g. Aniline as an auxiliary fluid [52]. Thus, the knowledge of the VLE properties of this mixture plays an important role for numerous industrial applications.

Figure 9 shows the isobaric VLE of Water + Hydrazine at 0.1013 MPa from experiment [21,53,54], simulation and Peng-Robinson EOS. The mixture is azeotropic, having a temperature maximum. The azeotropic point is at $x_{\text{H2O}} \approx 0.41$ mol/mol. It should be noted that the experimental data by Uchida et al. [54] and by Lobry de Bruyn and Dito [53] differ somewhat from each other, especially near the azeotropic region, where the data by Lobry de Bruyn and Dito [53] lie above the data by Uchida et al. [54]. In the Water-rich region, these data have a reverse order. The experimental vapor pressure by Uchida et al. [54] at 388.25 K and $x_{\text{H2O}} = 0.6925$ mol/mol was taken to adjust the binary parameter of the molecular model ($\xi = 1.3$) and of the Peng-Robinson EOS ($k_{ij} = -0.1325$). Considering the substantial experimental uncertainties, the data sets from all three approaches agree very favorably.

6.2 Monomethylhydrazine + Water

Monomethylhydrazine as a pure fluid is used as a propellant for launching rockets and satellites. It has also many other important applications, such as Oxygen scavenger for boiler feedwater, starting material for dye intermediates, catalysis for polymerization reactions etc. [55]. To recover Monomethylhydrazine from aqueous solutions in order to obtain propellant grade material, VLE data of its aqueous mixture are needed.

Figure 10 depicts the VLE of Monomethylhydrazine + Water at ambient pressure. It can be seen that

the experimental data by Ferriol et al. [56] and by Cohen-Adad et al. [57] are quite similar, however, they differ near the azeotropic region. Like aqueous Hydrazine, this mixture is azeotropic, having a temperature maximum. In this case, the azeotropic point lies at $x_{\mathrm{CH3-N2H3}} \approx 0.25$ mol/mol. The experimental data by Ferriol et al. [56] at 372.55 K and $x_{\mathrm{CH3-N2H3}} = 0.476$ mol/mol were taken to adjust the binary parameter of the molecular model ($\xi = 1.3$) and of the Peng-Robinson EOS ($k_{ij} = -0.197$). In the Water-rich region, to the left of the azeotropic point in Figure 10, VLE simulations were not feasible, because of sampling problems. Considering the substantial experimental uncertainties, the data sets from all three approaches agree very favorably.

6.3 Dimethylhydrazine + Water

Dimethylhydrazine is primarily used as a component of jet and rocket fuels. Other applications include it as an intermediate for chemical synthesis, as a stabilizer for organic peroxide fuel additives, as an absorbent for acid gases or as a plant growth control agent [58]. In the production of Dimethylhydrazine, aqueous solutions, containing usually 10 % to 40 % Dimethylhydrazine, are initially obtained. The design of distillation processes for separating Dimethylhydrazine from aqueous solution requires VLE data for the binary system Dimethylhydrazine + Water [59].

Figure 11 shows the isobaric VLE of Dimethylhydrazine + Water at 0.1013 MPa from experiment, simulation and Peng-Robinson EOS. In contrast to the the previous two binary systems, this mixture is zeotropic. The experimental data by Carleton [59] and by Ferriol et al. [56] are very similar, however, the phase envelope reported by Carleton [59] is a little wider. The experimental vapor pressure by Ferriol et al. [56] at 345.17 K and $x_{\mathrm{(CH3)2-N2H2}} = 0.571$ mol/mol was taken to adjust the binary parameter of the molecular model ($\xi = 1.3$) and of the Peng-Robinson EOS ($k_{ij} = -0.285$) [51]. It can be seen in the Figure 11 that the results obtained by molecular simulation agree well with the experimental results on the saturated liquid line, but overestimate the Dimethylhydrazine content on the saturated vapor line for intermediate compositions. In the Water-rich region and in the Dimethylhydrazine-rich region, the narrow two-phase envelope is well predicted by simulation, whereas the Peng-Robinson EOS yields a qualitatively different form.

16

6.4 Dimethylhydrazine + Hydrazine

Different mixtures of Hydrazine and Dimethylhydrazine, e.g. known as Aerozine 50 or UH25, are in wide use as rocket fuels [60]. Such mixtures are more stable than pure Hydrazine and have a higher density and boiling point than pure Dimethylhydrazine. The thermodynamic properties of such mixtures are of major importance for research, development and design efforts concerning their use as propellants or hydraulic working fluids in space propulsion systems [60].

The VLE of Dimethylhydrazine + Hydrazine is presented in Figure 12 at ambient pressure. This system is zeotropic. The experimental vapor pressure by Pannetier and Mignotte [61] at 346.35 K and $x_{(CH3)2-N2H2}$ = 0.4717 mol/mol was taken to adjust the binary parameter of the molecular model ($\xi = 1.01$) and of the Peng-Robinson EOS ($k_{ij} = -0.1$). It should be noted that the description of the interactions between LJ sites of unlike molecules was in this case very close to the standard Lorentz-Berthelot combining rules. It can be seen that simulation results match almost perfectly with the experimental data on the saturated liquid line. On the saturated vapor line, the experimental data and the simulation results exhibit some scatter, but the agreement is reasonable. The Peng-Robinson EOS yields a qualitatively different form.

6.5 Binary mixtures with Ammonia

The addition of a small amount of Ammonia to Hydrazine improves its performance in propulsion systems, such as the rocket internal combustion engine [62]. The high octane rating of Ammonia allows the compression to be higher than in case of pure Hydrazine, which is highly prone to detonation, while Hydrazine offsets drawbacks of Ammonia like high ignition point and low burn speed. An accurate investigation of the fluid phase behavior is therefore of interest.

Binary VLE of Ammonia with the three hydrazines are presented in Figure 13 for different temperatures. The experimental data by Chang et al. [62] at the highest vapor pressure for each system were taken to adjust the binary parameter of the molecular models ($\xi = 1.084$ for Hydrazine, $\xi = 1.016$ for Monomethyl-hydrazine and $\xi = 0.94$ for Dimethylhydrazine) and of the Peng-Robinson EOS ($k_{ij} = 0.055$ for Hydrazine, $k_{ij} = 0.0$ for Monomethylhydrazine, $k_{ij} = 0.07$ for Dimethylhydrazine).

It can be seen in the Figure 13 that Peng-Robinson EOS matches very well with the experimental data

for Hydrazine and Monomethylhydrazine. For Dimethylhydrazine, some deviations of the Peng-Robinson EOS from the experimental data at 293 K in the Dimethylhydrazine-rich region are present, which are attributed to the misfit of the pure substance vapor pressure.

The results obtained by molecular simulation match very well with the experimental data at the different temperatures for Monomethylhydrazine, yielding a mean unsigned error of about 4.0 %. For Dimethylhydrazine, the simulation results agree excellently with the experimental results at 253 and 293 K, differing by only about 0.2 % and 0.7 %, respectively, but they deviate from the experimental value at 273 K and $x_{\mathrm{NH3}} = 0.396$ mol/mol by about 11.8%. The simulation results for Hydrazine are in reasonable agreement with the experiment, yielding a mean unsigned error of about 7.3 %.

7 Henry's law constant

Practical challenges in pressurizing, storing and pumping liquid propellants, like Hydrazine and its derivatives, require accurate data on the insolubility of ordinary gases [63]. However, absorption and desorption of these gases may cause undesirable mechanical and hydrodynamical effects in space vehicles [62]. Therefore, the solubility of a gas in these propellants should be small enough to permit its use as a pressurant in rocket booster engines [62].

On the basis of the newly developed molecular models, the Henry's law constant for the most important propellant pressurization gases Ar, N_2 and CO in the pure liquid hydrazines were predicted and compared with the experimental data by Chang et al. [62,63], which is the sole publicly available source. For CO, the Henry's law constant was calculated only in liquid Dimethylhydrazine, because no experimental data were available for the other two hydrazines.

Here, a straightforward route as described in [49] was followed. The Henry's law constant H_i is related to the residual chemical potential of the solute i at infinite dilution in the solvent μ_i^∞ [29,64] by

$$H_i = \rho_s k_{\mathrm{B}} T \exp\left(\mu_i^\infty / (k_{\mathrm{B}} T)\right), \tag{11}$$

where ρ_s is the density of the solvent in its saturated liquid state.

The Henry's law constant is hence directly related to the unlike solvent-solute interaction and indirectly

to the like solvent-solvent interaction, which yields the configurations of the solvent molecules and is fully given by the solvent model. To define the unlike LJ contribution between solute i and solvent molecules, the modified Lorentz-Berthelot combining rule, as described by equations (2) and (4), was used.

It should be noted that the Henry's law constant decreases with increasing binary interaction parameter ξ, i.e. the solubility is enhanced due to stronger unlike dispersive attraction [29,49]. Here, the binary interaction parameter ξ was adjusted to the experimental Henry's law constant data at the highest or at the lowest temperature for which binary experimental data exist. The temperature dependence that was obtained from simulation is thus a fully predictive property.

Figure 14 shows the predicted Henry's law constant H_i in liquid Hydrazine, Monomethylhydrazine and Dimethylhydrazine in comparison to experimental data. All present data are given in numerical form in the supplementary material. Linear functions are sufficient to represent the data. It can be seen that the order of magnitude and also the temperature dependence of H_i vary very strongly for these systems. E.g., H_i ranges from around 10 to 20 GPa for Ar and N_2 in Hydrazine to around 0.1 to 0.3 GPa for the same gases in Dimethylhydrazine. Moreover, it strongly decreases with the temperature in the first case, but changes little with temperature in the second case.

The average deviation from the experimental gas solubility data for Hydrazine is about 3.7% for Ar and 3.9% for N_2. The results obtained with the Monomethylhydrazine model overestimate the available experimental data by about 2.5% for Ar and 1.3% for N_2. For the Dimethylhydrazine model, the achieved agreement is also excellent, yielding a mean unsigned error of about 0.5% for Ar, 2.3% for N_2 and 1.7% for CO.

8 Discussion of the binary interaction parameter of the molecular models

In this work, a total of 14 binary mixtures containing hydrazines was studied. It should be noted that the adjusted binary interaction parameter, that acts between LJ sites of unlike molecule type is close to the standard Lorentz-Berthelot combining rules (ξ=1), except for the aqueous systems. Table 4 lists all binary parameters. These values are in the range that was found for ξ in preceding work of our group [65] regarding 267 other binary mixtures.

For all systems containing water, the binary interaction parameter is the same (ξ=1.3) and differs quite strongly from the value ξ=1 that would be used for strictly predictive applications. As noticed by Huang et al. [37], this can be explained by the fact that the interactions of water are dominated by electrostatics and the comparably weak unlike dispersive interaction has to be modified significantly to adjust the mixture model.

9 Conclusion

Molecular modeling and simulation was applied to predict the phase behavior of pure fluids and binary mixtures containing Hydrazine and two of its derivatives. New molecular models were developed for Hydrazine, Monomethylhydrazine and Dimethylhydrazine, partly based on quantum chemical information on molecular geometry and electrostatics. Furthermore, experimental data on the saturated liquid density and the vapor pressure were taken into account to optimize the pure substance models. These pure substance properties were represented accurately from the triple point to the critical point. It was also shown that the Hydrazine model is capable to properly predict the second virial coefficient and the density of homogeneous liquid Hydrazine, while no experimental data for these properties were used in the optimization procedure. Unfortunately, no experimental data on these properties were available for Monomethylhydrazine. The density of homogeneous liquid Dimethylhydrazine was also excellently predicted over a wide temperature range. The second virial coefficient of Monomethylhydrazine and Dimethylhydrazine was predicted, however, no other data were available for comparison. The new models were compared with molecular models by Gutowski et al. [5] and were found to yield more reliable results for most thermodynamic properties.

For an optimized description of the binary VLE, the unlike dispersive interaction was adjusted for all 14 studied binary systems to a single experimental vapor pressure of the mixture in the vicinity of ambient conditions. With these binary mixture models, VLE data were predicted for a temperature and composition range. The predictions show a good agreement with experimental binary VLE data that were not considered in the model development. The simulations also confirm that Hydrazine and its derivatives are very dissimilar fluids. E.g., Dimethylhydrazine does not form an azeotrope with Water, while the other

two hydrazines do form an azeotrope. Moreover, the Henry's law constant of Argon, Nitrogen and Carbon Monoxide has a different order of magnitude and a different temperature dependence in these liquids.

In this work, molecular modeling and simulation was used to predict the fluid phase behavior and the thermodynamic properties of pure hydrazines and binary hydrazine mixtures, for which experimental data were available for comparison. The presented molecular models were able to well reproduce the experimental data that were not considered in the model development. Thus, these new models could also be valuable for the prediction of properties under different conditions and for systems, where no experimental data are available.

Acknowledgements

10   Appendix: Simulation details

The Grand Equilibrium method [66] was used to calculate VLE data for all systems and the calculations were performed with the $ms2$ simulation code [67]. For the liquid, Monte-Carlo simulations were performed in the isobaric-isothermal (NpT) ensemble. There, the number of molecules was 800 for pure fluids and 864 for mixtures. The gradual insertion method [68,69] was used to calculate the chemical potential for all binary systems with Water. For all other binary systems, Widom's insertion method [70] was used. Starting from a face centered cubic lattice, 30 000 Monte Carlo cycles with the first 10 000 cycles in the canonical (NVT) ensemble were performed for equilibration and 100 000 for production. Each cycle contained a number of attempts to displace and rotate molecules equal to the actual number of molecules N plus one

volume move. Every cycle, $10 \times N$ fluctuating state change moves, $10 \times N$ fluctuating particle transla-tion/rotation moves, and $50 \times N$ biased particle translation/rotation moves were sampled to determine the chemical potential. For the corresponding vapor, Monte Carlo simulations in the pseudo-μVT ensemble were performed. The simulation volume was adjusted to lead to an average number of 500 molecules in the vapor phase. After 10 000 initial NVT Monte Carlo cycles, starting from a face centered cubic lattice, 25 000 equilibration cycles in the pseudo-μVT ensemble were sampled. The length of the production run was 100 000 cycles. The cut-off radius was set to 15 Å throughout and a center of mass cut-off scheme was employed. Lennard-Jones long-range interactions beyond the cut-off radius were corrected employing angle averaging as proposed by Lustig [71]. Electrostatic interactions were calculated using the reaction field method [11]. Statistical uncertainties of the simulated values were estimated by a block averaging method [72].

To calculate the Henry's law constant, the residual chemical potential of a component at infinite dilution μ_i^∞ was evaluated using Widom's method. The mole fraction of the solute in the solvent was exactly zero, as required for infinite dilution. MD simulations were performed in the liquid state at a specified temperature and the pressure was set to the pure substance vapor pressure of the solvent, as described by the molecular model. Therefore, test molecules representing the solute i were inserted into the pure saturated liquid solvent after each time step at random spatial coordinates and orientations, and the potential energy ψ_i between the solute test molecule i and all solvent molecules was calculated within the cut-off radius. Thus only solute-solvent interactions were sampled. The number of test molecules was 3456. The residual chemical potential at infinite dilution μ_i^∞ was then obtained by

$$\mu_i^\infty = -k_{\mathrm{B}}T \ln \langle V \exp\left(-\psi_i/(k_{\mathrm{B}}T)\right)\rangle/\langle V \rangle, \tag{12}$$

where V is the volume and the brackets represent the NpT ensemble average.

Transport properties were determined by equilibrium MD simulations following the Green-Kubo formalism [73,74]. For that task, MD Simulation were performed in two steps. In the first step, a simulation in the NpT ensemble was performed at the desired temperature and pressure to obtain the density. The system was equilibrated over 70 000 time steps, thereof 20 000 in the NVT ensemble, followed by a production run of 500 000 time steps. In the second step, a NVT ensemble simulation was performed at this temperature

and density to calculate the transport properties. The simulations were equilibrated in the NVT ensemble over 100 000 time steps, followed by production runs of 1 000 000 time steps. The shear viscosity was calculated with 5000 independent time origins of the autocorrelation functions. The sampling length of the autocorrelation functions was 2000 time steps. The separation between the time origins was chosen such that all autocorrelation functions have decayed at least to $1/e$ of their normalized value to guarantee their time independence [75].

References

[1] K. Khachaturyan, Nauka i Zhizn (USSR) 1 (1999) 48-56 and 3 (1999) 52-58.

[2] http://www.aerospaceweb.org/question/spacecraft/q0179.shtml

[3] http://www.russianspaceweb.com/r16_disaster.html

[4] G.E. Collins, S.L. Rose-Pehrsson, Analyst 119 (1994) 1907-1913.

[5] K.E. Gutowski, B. Gurkan, E.J. Maginn, Pure Appl. Chem. 81 (2009) 1799-1828.

[6] E.W. Schmidt, Hydrazine and its Derivatives: Preparation, Properties, Applications, Wiley, New York, 1984.

[7] R. Von Burg, T. Stout, J. Appl. Toxicol. 11 (1991) 447-450.

[8] O. Borodin, J. Phys. Chem. B 113 (2009) 11463-11478.

[9] J.E. Jones, Proc. Roy. Soc. 106A (1924) 441-462.

[10] J.E. Jones, Proc. Roy. Soc. 106A (1924) 463-477.

[11] M.P. Allen, D.J. Tildesley, Computer simulations of liquids, Oxford University Press, Oxford, 1987.

[12] C.G. Gray, K.E. Gubbins, Theory of molecular fluids. 1. Fundamentals, Clarendon Press, Oxford, 1984.

[13] C. Engin, J. Vrabec, H. Hasse, Mol. Phys. 109 (2011) 1975-1982.

[14] H.A. Lorentz, Ann. d. Phys. 12 (1881) 127-136.

[15] D. Berthelot, Compt. Rend. Ac. Sc. 126 (1898) 1703-1706.

[16] M.W. Schmidt, K.K. Baldridge, J.A. Boatz, S.T Elbert, M.S. Gordon, J.H. Jensen, S. Koseki, N. Matsunaga, K.A. Nguyen, S. Shujun, T.L. Windus, M. Dupuis, A.M. Montgomery, J. Comput. Chem. 14 (1993) 1347-1363.

[17] T. Schnabel, J. Vrabec, H. Hasse, Fluid Phase Equilib. 263 (2008) 144-159.

[18] T. Merker, J. Vrabec, H. Hasse, Soft Materials 10 (2012) 3-24.

[19] A. Kaczmarek, M. Shiga, D. Marx, J. Phys. Chem. A 113 (2009) 1985-1994.

[20] W.A. Seddon, J.W. Fletcher, F.C. Sopchyshyn, Can. J. Chem. 54 (1976) 2807-2812.

[21] Dortmunder Datenbank, Mixture Properties, Version 6.3.0.384 (2010).

[22] R.L. Rowley, W.V. Wilding, J.L. Oscarson, Y. Yang, N.A. Zundel, T.E. Daubert, R.P. Danner, DIPPR Information and Data Evaluation Manager for the Design Institute for Physical Properties, AIChE, New York, Version 5.0.2 (2011).

[23] A. Lotfi, J. Vrabec, J. Fischer, Mol. Phys. 76 (1992) 1319-1333.

[24] G. Hradetzky, D.A. Lempe, Merseburg Data Bank MDB for thermophysical data of pure compounds, Revision 7.1.0. (2010).

[25] J.L. Haws, D.G. Harden, J. Spacecr. Rockets 2 (1965) 972-974.

[26] L.F. Audrieth, B. Ackerson Ogg, The Chemistry of Hydrazine, John Wiley, New York, 1951.

[27] R.S. Drago, H.H. Sisler, J. Phys. Chem., 60 (1956) 245-249.

[28] C. Tsonopoulos, AIChE J. 24 (1978) 1112-1115.

[29] T. Schnabel, J. Vrabec, H. Hasse, Fluid Phase Equilib. 233 (2005) 134-143.

[30] J. Vrabec, J. Stoll, H. Hasse, J. Phys. Chem. B 105 (2001) 12126-12133.

[31] W. Beamer, J. Am. Chem. Soc. 70 (1948) 2979-2982.

[32] J.G. Aston, J.L. Wood, T.P. Zolki, J. Am. Chem. Soc. 75 (1953) 6202-6204.

[33] J. Stoll, J. Vrabec, H. Hasse, J. Chem. Phys. 119 (2003) 11396-11407.

[34] B. Eckl, J. Vrabec, H. Hasse, Mol. Phys. 106 (2008) 1039-1046.

[35] W.L. Jorgensen, J.D. Chandrasekhar, R.W. Madura, R.W. Impey, M.L. Klein, J. Chem. Phys. 79 (1983) 926-935.

[36] C. Vega, J.L.F Abascal, Phys. Chem. Chem. Phys. 13 (2011) 19663-19688.

[37] Y.-L. Huang, T. Merker, M. Heilig, H. Hasse, J. Vrabec, Ind. Eng. Chem. Res., submitted 2011.

[38] Y.-L. Huang, PhD thesis, University of Paderborn, 2010.

[39] H.W. Horn, W.C. Swope, J.W. Pitera, J.D. Madura, T.J. Dick, G.L. Hura, T. Head-Gordon, J. Chem. Phys. 120 (2004) 9665-9678.

[40] J.L.F. Abascal, C. Vega, J. Chem. Phys. 123 (2005) 234505-234516.

[41] J.L.F. Abascal, E. Sanz, R. García Fernández, C. Vega, J. Chem. Phys. 122 (2005) 234511-234519.

[42] Y. Guissani, B. Guillot, J. Chem. Phys. 98 (1993) 8221-8235.

[43] T. Schnabel, J. Vrabec, H. Hasse, J. Mol. Liq. 135 (2007) 170-178.

[44] J. Stoll, Fortschritt-Berichte VDI, Reihe 3, Vol. 836, VDI-Verlag, Düsseldorf, 2005.

[45] J. Stoll, J. Vrabec, H. Hasse, AIChE J. 49 (2003) 2187-2198.

[46] J. Vrabec, J. Stoll, H. Hasse, Mol. Sim. 31 (2005) 215-221.

[47] J. Carrero-Mantilla, M. Llano-Restrepo, Mol. Sim. 29 (2003) 549-554.

[48] G. Guevara-Carrion, H. Hasse, J. Vrabec, Top. Curr. Chem. 307 (2012) 201-250.

[49] Y.-L. Huang, S. Miroschnichenko, H. Hasse, J. Vrabec, Int. J. of Thermophys. 30 (2009) 1791-1810.

[50] J.M. Smith, H.C. Van Ness, M.M. Abbott, Introduction to chemical engineering thermodynamics, fifth ed, New York: McGraw-Hill, 1996.

[51] D.Y. Peng, D.B. Robinson, Ind. Eng. Chem. Fundam. 15 (1976) 59-64.

[52] www.atsdr.cdc.gov/ToxProfiles/tp100-c4.pdf

[53] C.A. Lobry de Bruyn, J.W. Dito, Proc. Sec. Sci./K. Akad. Wet. Amsterdam 5 (1902-1903) 171-183.

[54] S. Uchida, S. Ogawa, M. Yamaguchi, Jap. Sci. Rev. Eng. Sci. 1 (1950) 41-49.

[55] S. Sridhar, R. Ravindra, A.A. Khan, Ind. Eng. Chem. Res. 39 (2000) 2485-2490.

[56] M. Ferriol, A. Laachach, M.T. Cohen-Adad, F.W. Getzen, L. Jorat, G. Noyel, J. Huck, J.C. Bureau, Fluid Phase Equilib. 71 (1992) 287-299.

[57] M.T. Cohen-Adad, I. Allali, F.W. Getzen, J. Solution Chem. 16 (1987) 659-678.

[58] U.S. Environmental Protection Agency. Health and Environmental Effects Profile for 1,1-Dimethylhydrazine. EPA/600/x-84/134. Environmental Criteria and Assessment Office, Office of Health and Environmental Assessment, Office of Research and Development, Cincinnati, OH, 1984.

[59] L.T. Carleton, Ind. Eng. Chem. Chem. Eng. Data Series 1 (1956) 21-24.

[60] J.P. Copeland, J.A. Simmons, J.M. Spurlock, Phase I Report for Manned Spacecraft Center, National Aeronautics and Space Administration, Atlantic Research Corporation, 1967.

[61] G. Pannetier, P. Mignotte, Bull. Soc. Chim. Fr. 143 (1961) 985-988.

[62] E.T. Chang, N.A. Gokcen, T.M. Poston, J. Chem. Eng. Data 16 (1971) 404-408.

[63] E.T. Chang, N.A. Gokcen, T.M. Poston, J. Phys. Chem. 72 (1968) 638-642.

[64] K.S. Shing, K.E. Gubbins, K. Lucas, Mol. Phys. 65 (1988) 1235-1252.

[65] J. Vrabec, Y.-L. Huang, H. Hasse, Fluid Phase Equilib. 279 (2009) 120-135.

[66] J. Vrabec, H. Hasse, Mol. Phys. 100 (2002) 3375-3383.

[67] S. Deublein, B. Eckl, J. Stoll, S.V. Lishchuk, G. Guevara-Carrion, C.W. Glass, T. Merker, M. Bernreuther, H. Hasse, J. Vrabec, Comp. Phys. Commun. 182 (2011) 2350-2367.

[68] I. Nezbeda, J. Kolafa, Mol. Sim. 5 (1991) 391-403.

[69] J. Vrabec, M. Kettler, H. Hasse, Chem. Phys. Lett. 356 (2002) 431-436.

[70] B. Widom, J. Chem. Phys. 39 (1963) 2808-2812.

[71] R. Lustig, Mol. Phys. 65 (1988) 175-179.

[72] H. Flyvbjerg, H.G. Petersen, J. Chem. Phys. 91 (1989) 461-466.

[73] M.S. Green, J. Chem. Phys. 22 (1954) 398-413.

[74] R. Kubo, J. Phys. Soc. Jpn. 12 (1957) 570-586.

[75] M. Schoen, C. Hoheisel, Mol. Phys. 52 (1984) 33-56.

[76] NIST Standard Reference Database 23, Programm REFPROP (REFerence fluid PROPerties), Version 8.0, 2007.

[77] E.A. Guggenheim, J. Chem. Phys. 13 (1945) 253-261.

Table 1
Parameters of the molecular models for Hydrazine, Monomethylhydrazine and Dimethylhydrazine developed in this work. Lennard-Jones interaction sites are denoted by the modeled atomic groups. Electrostatic interaction sites are denoted by point charge. Coordinates are given with respect to the center of mass in a principal axes system.

interaction site	x	y	z	σ	ϵ/k_B	q
	Å	Å	Å	Å	K	e
Hydrazine						
NH$_2$	0.044	−0.062	0.705	3.3523	146.41	
NH$_2$	0.044	0.062	−0.705	3.3523	146.41	
point charge (N)	0.044	−0.062	0.705			−0.6616
point charge (H1)	0.271	0.869	1.076			0.3308
point charge (H2)	−0.892	−0.307	1.062			0.3308
point charge (N)	0.044	0.062	−0.705			−0.6616
point charge (H1)	−0.893	0.305	−1.062			0.3308
point charge (H2)	0.274	−0.869	−1.076			0.3308
Monomethylhydrazine						
CH$_3$	−0.025	−0.302	1.477	3.6072	120.15	
NH	0.043	0.597	0.036	3.3587	147.83	
NH$_2$	−0.057	−0.305	−1.075	3.3587	147.83	
point charge (N)	−0.057	−0.305	−1.075			−0.6654
point charge (H1)	0.856	−0.705	−1.308			0.3327
point charge (H2)	−0.361	0.244	−1.875			0.3327
Dimethylhydrazine						
CH$_3$	−0.155	1.312	0.904	3.6072	120.15	
CH$_3$	−0.164	−1.316	0.910	3.6072	120.15	
N	0.395	−0.053	0.197	3.3211	34.90	
NH$_2$	−0.081	0.070	−1.496	3.3085	141.15	
point charge (N)	−0.081	0.070	−1.496			−0.6882
point charge (H1)	0.497	−0.609	−1.990			0.3441
point charge (H2)	−1.056	−0.251	−1.590			0.3441

Table 2
Critical properties on the basis of the present molecular models in comparison to experimental data.

substance	T_c^{sim}	T_c^{exp}	ρ_c^{sim}	ρ_c^{exp}	p_c^{sim}	p_c^{exp}	Exp.
	K	K	mol/l	mol/l	MPa	MPa	Ref.
Hydrazine	647.6	653	10.16	10.41	13.04	14.69	[21]
Hydrazine	647.6	653.15	10.16	6.33	13.04	14.69	[22,24]
Hydrazine	647.6	653	10.16	7.18	13.04	14.69	[6,25,26]
Monomethylhydrazine	606.6	567	6.53	3.69	7.66	8.04	[21]
Monomethylhydrazine	606.6	567	6.53	3.69	7.66	8.24	[24]
Monomethylhydrazine	606.6	585	6.53	6.29	7.66	8.21	[6]
Dimethylhydrazine	514.5	523	4.95	4.58	5.00	5.40	[6]

Table 3
Pure substance parameters of the Peng-Robinson EOS, taken from [5,21,76] and derived from the present simulation results for Dimethylhydrazine.

substance	T_c	p_c	ω	M
	K	MPa	-	g/mol
Hydrazine	653.0	14.69	0.3280	32.050
Monomethylhydrazine	567.0	8.04	0.3901	46.072
Dimethylhydrazine	523.0	5.00	0.2861	60.100
Ammonia	405.4	11.33	0.2560	17.030
Water	647.3	22.05	0.3440	18.015

Table 4
Binary interaction parameters of the molecular models and binary parameters of the Van der Waals one-fluid mixing rule of the Peng-Robinson equation of state as adjusted in the present work.

Mixture	ξ	k_{ij}
Water + Hydrazine	1.3	-0.1325
Monomethylhydrazine + Water	1.3	-0.197
Dimethylhydrazine + Water	1.3	-0.285
Dimethylhydrazine + Hydrazine	1.01	-0.1
Ammonia + Hydrazine	1.084	0.055
Ammonia + Monomethylhydrazine	1.016	0.0
Ammonia + Dimethylhydrazine	0.94	0.07
Argon + Hydrazine	1.02	$-$
Nitrogen + Hydrazine	1.11	$-$
Argon + Monomethylhydrazine	0.933	$-$
Nitrogen + Monomethylhydrazine	0.976	$-$
Argon + Dimethylhydrazine	0.945	$-$
Nitrogen + Dimethylhydrazine	0.955	$-$
Carbone Monoxide + Dimethylhydrazine	1.005	$-$

List of Figures

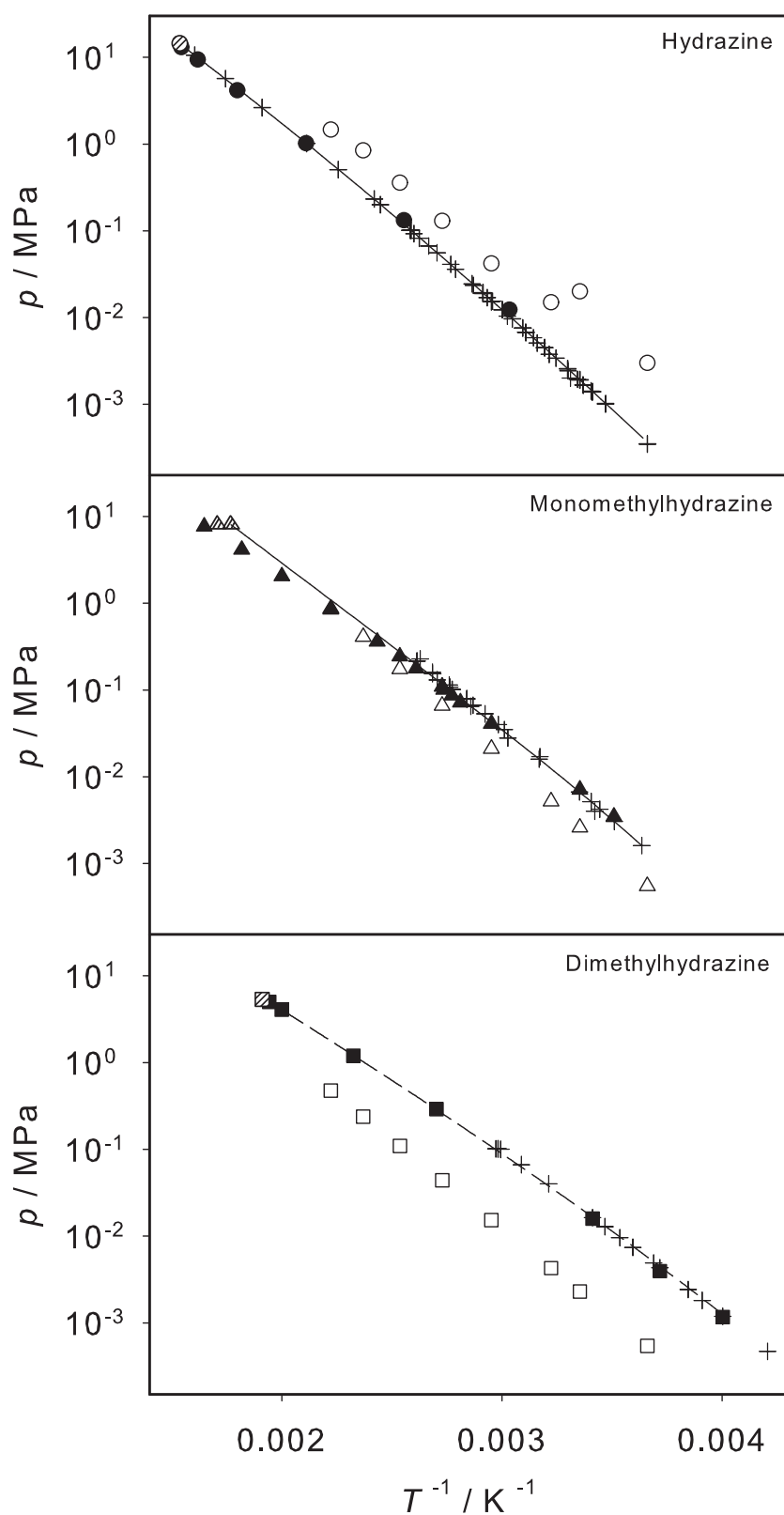Fig. 1. Saturated densities of Hydrazine (●), Monomethylhydrazine (▲) and Dimethylhydrazine (■): (striped symbols) experimental critical data [5,21,22,24]; (+) experimental saturated liquid densities [21,22]; (full symbols) simulation data on the basis of the present models; (empty symbols) simulation data (saturated liquid only) by Gutowski et al. [5]; (——) correlation of experimental data [22]; (- - -) correlation of present simulation data [77]. The statistical uncertainties of the present data are within symbol size.
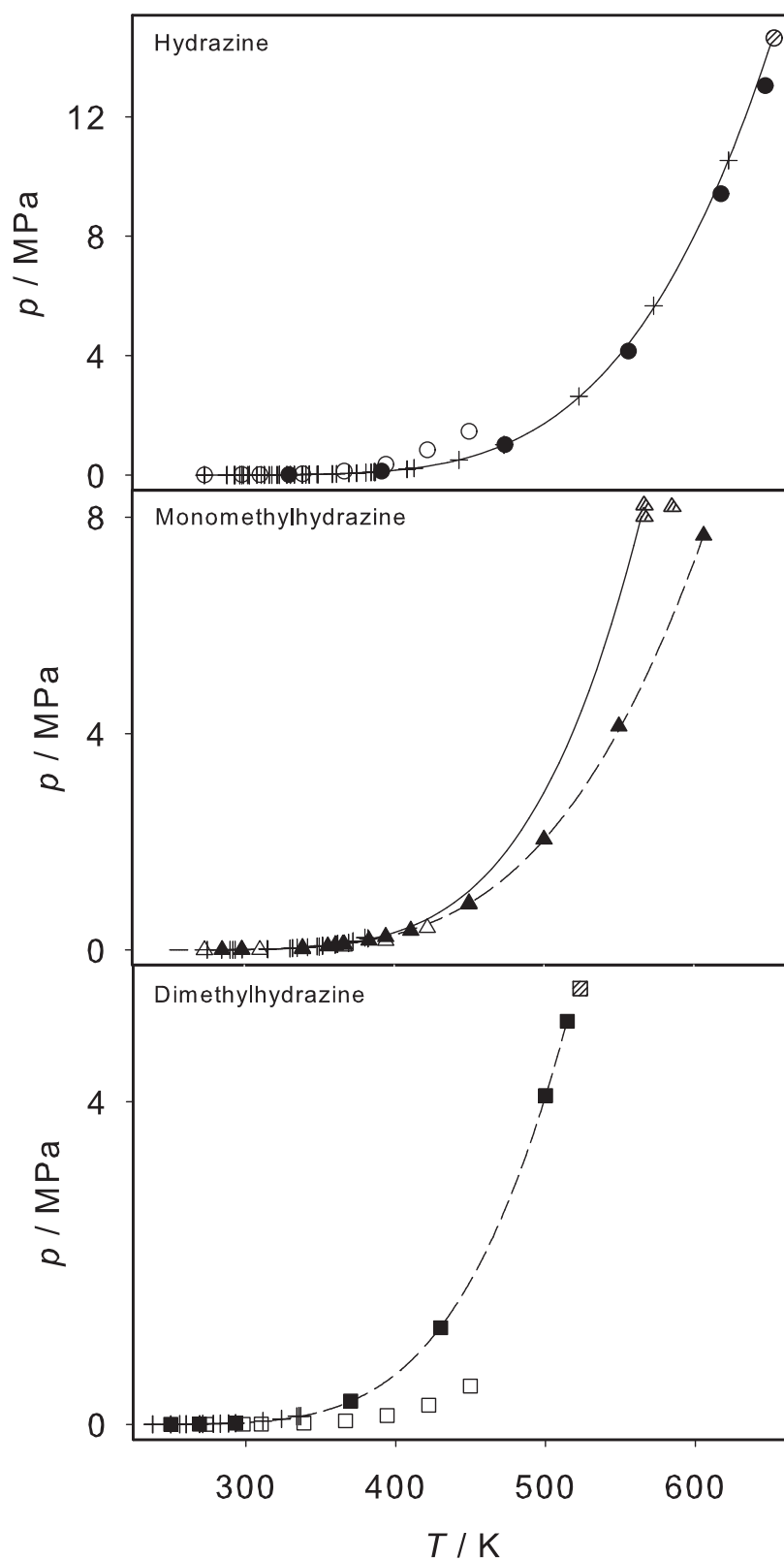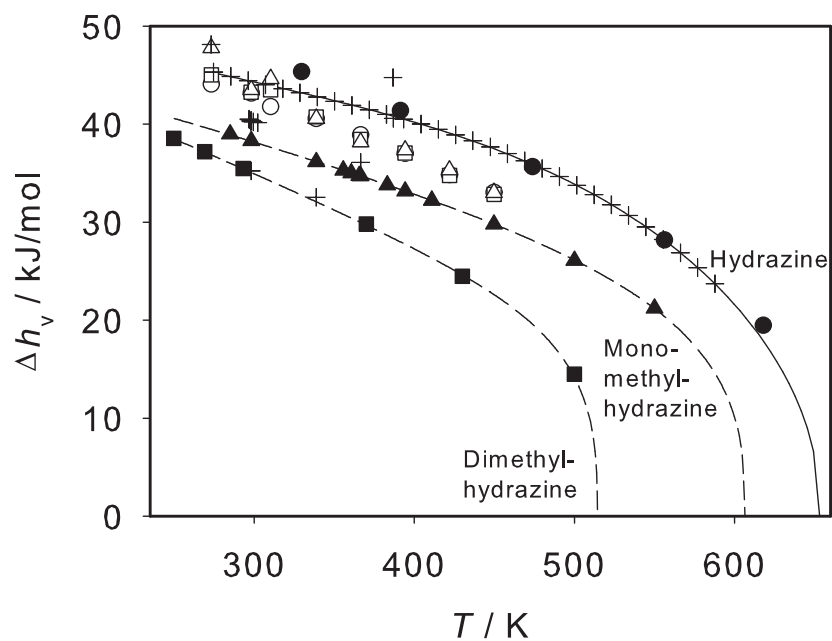
Fig. 2. Vapor pressure of Hydrazine (●), Monomethylhydrazine (▲) and Dimethylhydrazine (■): (striped symbols) experimental critical data [21,22,24]; (+) experimental data [21]; (full symbols) simulation data on the basis of the present models; (empty symbols) simulation data by Gutowski et al. [5]; (——) correlation of experimental data [22,24]; (- - -) correlation of present simulation data [77]. The statistical uncertainties of the present data are within symbol size.

Fig. 3. Logarithmic vapor pressure of Hydrazine (●), Monomethylhydrazine (▲) and Dimethylhydrazine (■): (striped symbols) experimental critical data [21,22,24]; (+) experimental data [21]; (full symbols) simulation data on the basis of the present models; (empty symbols) simulation data by Gutowski et al. [5]; (——) correlation of experimental data [24]; (- - -) correlation of present simulation data [77]. The statistical uncertainties of the present data are within symbol size.

Fig. 4. Enthalpy of vaporization of Hydrazine (●), Monomethylhydrazine (▲) and Dimethylhydrazine (■): (+) experimental data [21]; (full symbols) simulation data on the basis of the present models; (empty symbols) simulation data by Gutowski et al. [5]; (——) correlation of experimental data [22]; (- - -) correlation of present simulation data [77]. The statistical uncertainties of the present data are within symbol size.
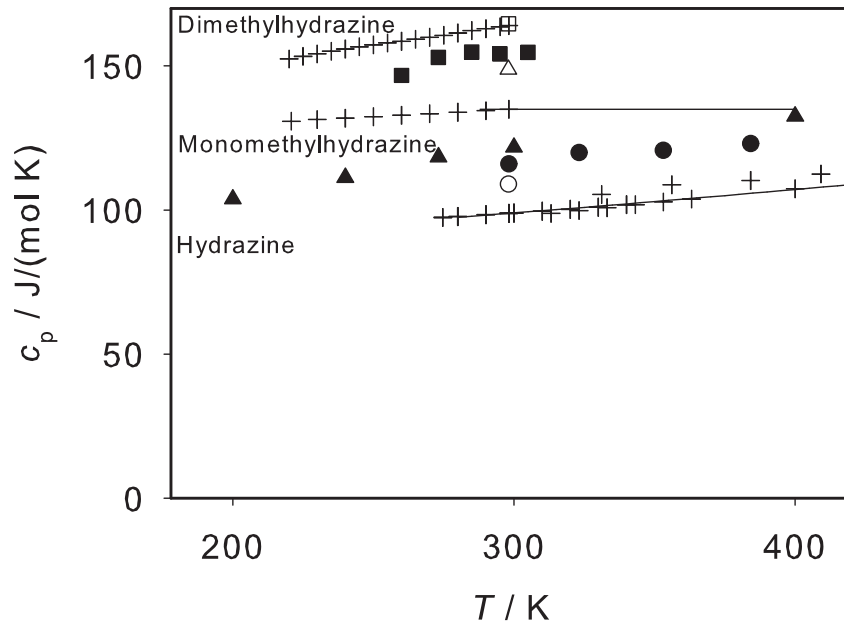
Fig. 5. Isobaric heat capacity of liquid Hydrazine (●), Monomethylhydrazine (▲) and Dimethylhydrazine (■) at 0.1013 MPa: (+) experimental data [21,22,32]; (full symbols) simulation data on the basis of the present models; (empty symbols) simulation data by Gutowski et al. [5]; (——) correlations of experimental data [22,24]. The statistical uncertainties of the present data are within symbol size.
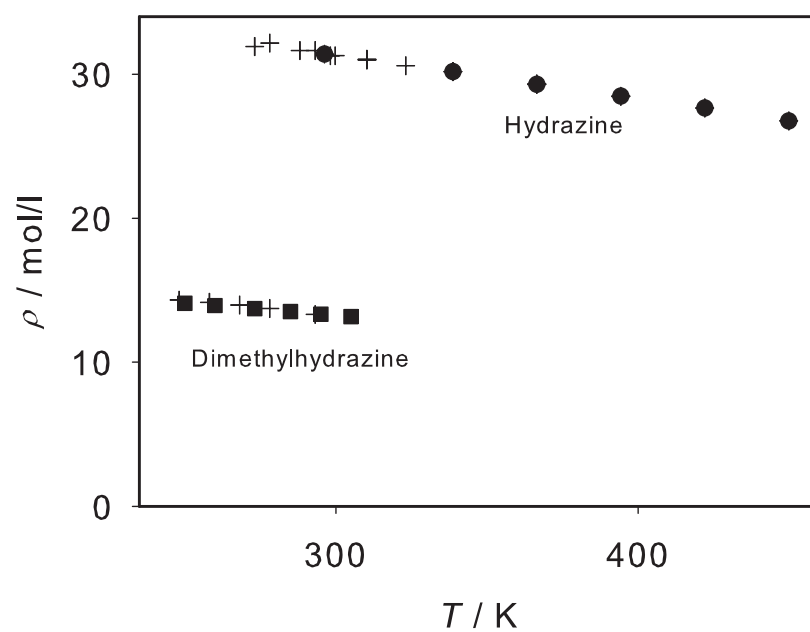
Fig. 6. Density of liquid Hydrazine (●) and Dimethylhydrazine (■) at 0.1013 MPa: (+) experimental data [21]; (full symbols) present simulation data. The statistical uncertainties of the present data are within symbol size.
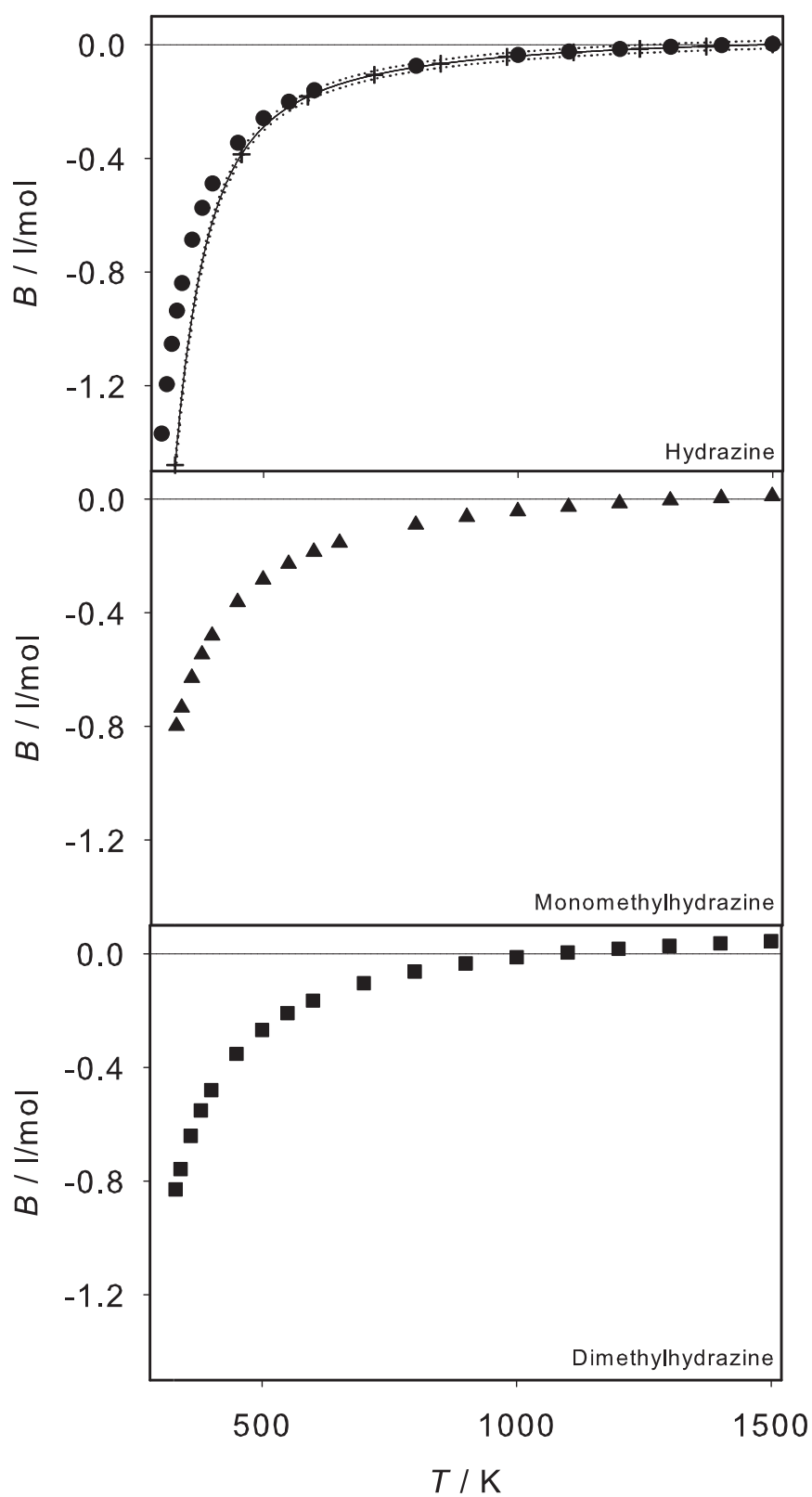
Fig. 7. Second virial coefficient of Hydrazine (●), Monomethylhydrazine (▲) and Dimethylhydrazine (■): (full symbols) present simulation data; (+) virial coefficients estimated with the method by Tsonopoulos [22,28], (——) correlation of estimated data [22,28]; (· · ·) uncertainty of the correlation.
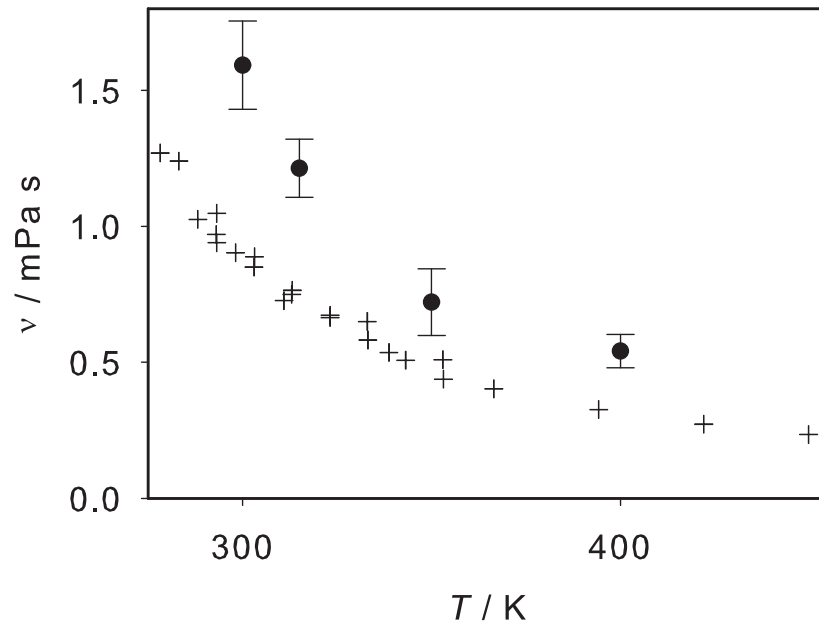
Fig. 8. Shear viscosity of liquid Hydrazine at 0.1013 MPa: (+) experimental data [21]; (●) present simulation data.
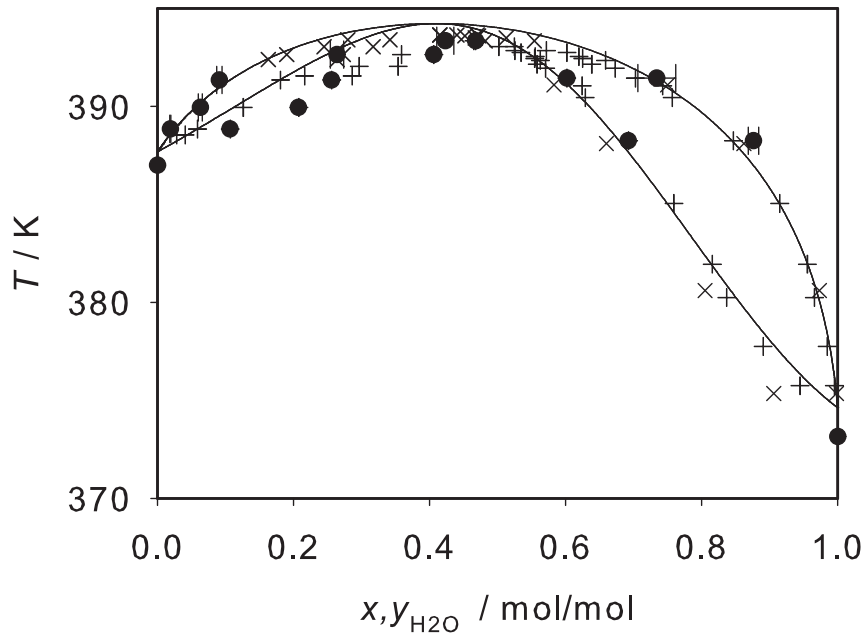
Fig. 9. Isobaric vapor-liquid phase diagram of Water + Hydrazine at 0.1013 MPa: ($\times$) experimental data by Lobry de Bruyn and Dito [53]; (+) experimental data by Uchida et al. [54]; ($\bullet$) present simulation data with ξ=1.3; (——) Peng-Robinson EOS with k_{ij}=−0.1325.
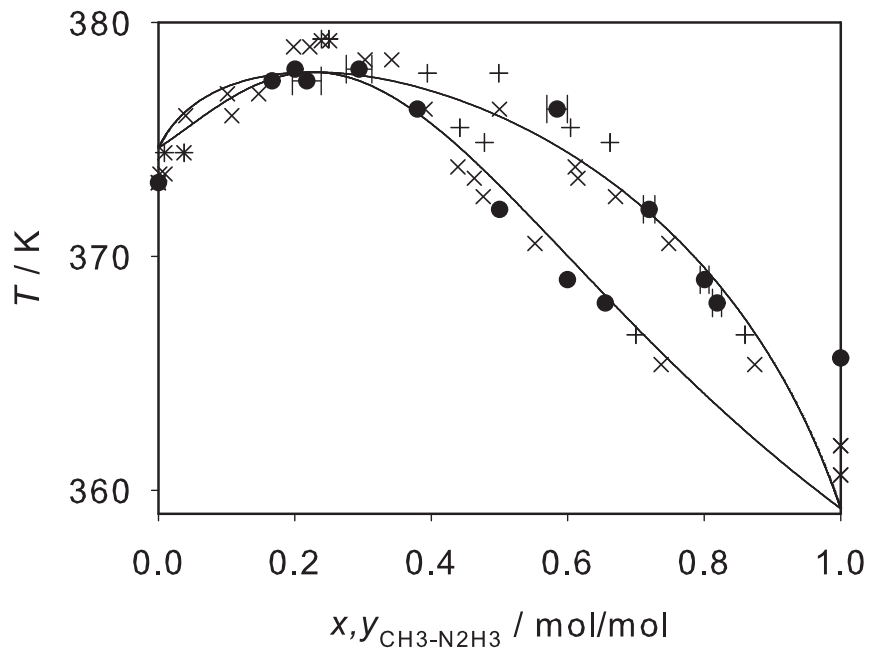
Fig. 10. Isobaric vapor-liquid phase diagram of Monomethylhydrazine + Water at 0.1013 MPa: ($\times$) experimental data by Ferriol et al. [56]; ($+$) experimental data by Cohen-Adad et al. [57]; ($\bullet$) present simulation data with $\xi=1.3$; (——) Peng-Robinson EOS with $k_{ij}=-0.197$.
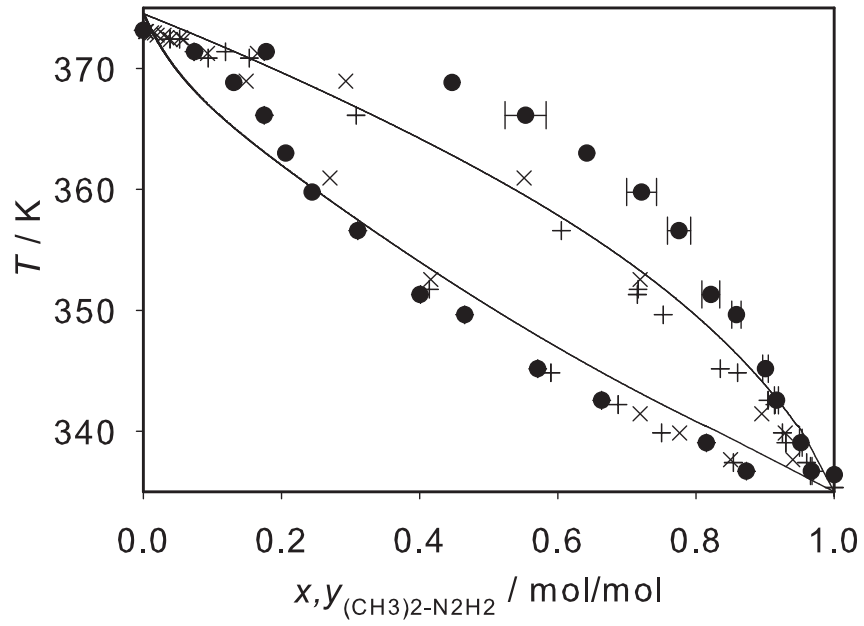
Fig. 11. Isobaric vapor-liquid phase diagram of Dimethylhydrazine + Water at 0.1013 MPa: (×) experimental data by Carleton [59]; + experimental data by Ferriol et al. [56]; (●) present simulation data with ξ=1.3; (——) Peng-Robinson EOS with k_{ij}=−0.285.
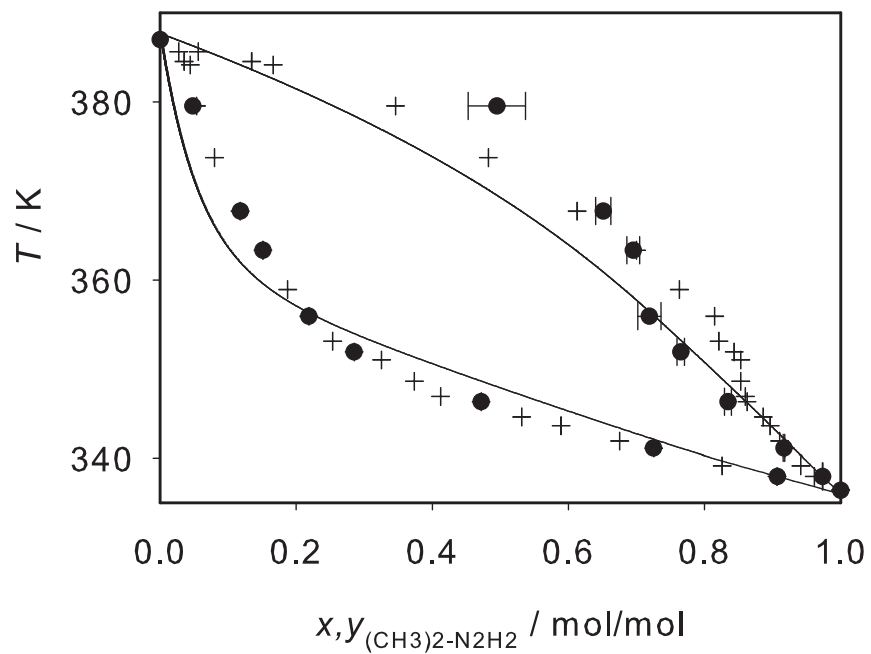
Fig. 12. Isobaric vapor-liquid phase diagram of Dimethylhydrazine + Hydrazine at 0.1013 MPa: (+) experimental data by Pannetier and Mignotte [61]; ($\bullet$) present simulation data with ξ=1.01; (——) Peng-Robinson EOS with k_{ij}=−0.1.
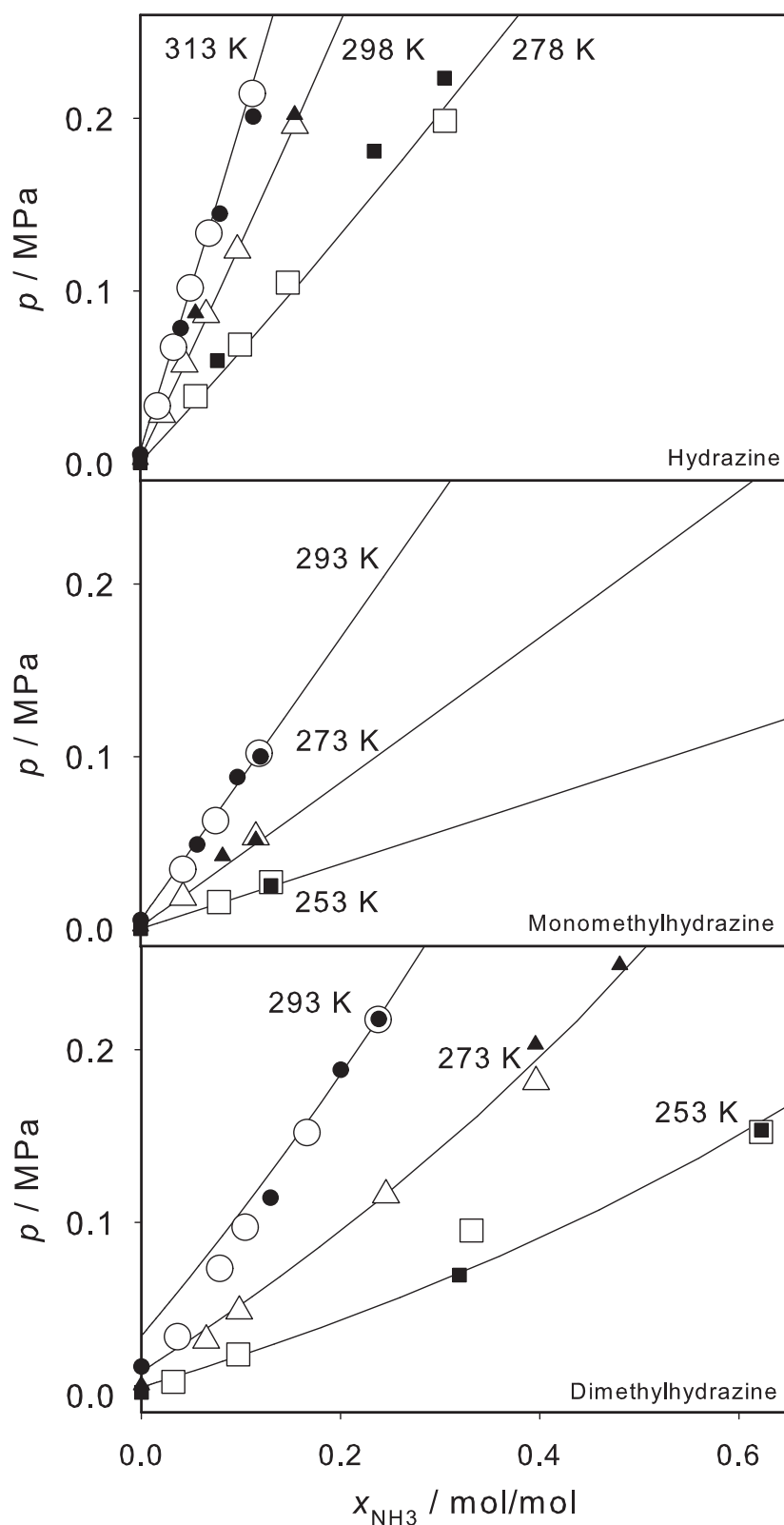
Fig. 13. Isothermal vapor-liquid phase diagrams of binary mixtures containing Ammonia and the hydrazines at different temperatures: (empty symbols) experimental data by Chang et al. [62]; (●) present simulation data with ξ=1.084 for Hydrazine, (▲) ξ=1.016 for Monomethylhydrazine, (■) ξ=0.94 for Dimethylhydrazine; (——) Peng-Robinson EOS with k_{ij}=0.055 for Hydrazine, k_{ij}=0.0 for Monomethylhydrazine, k_{ij}=0.07 for Dimethylhydrazine. The statistical uncertainties of the present data are within symbol size.
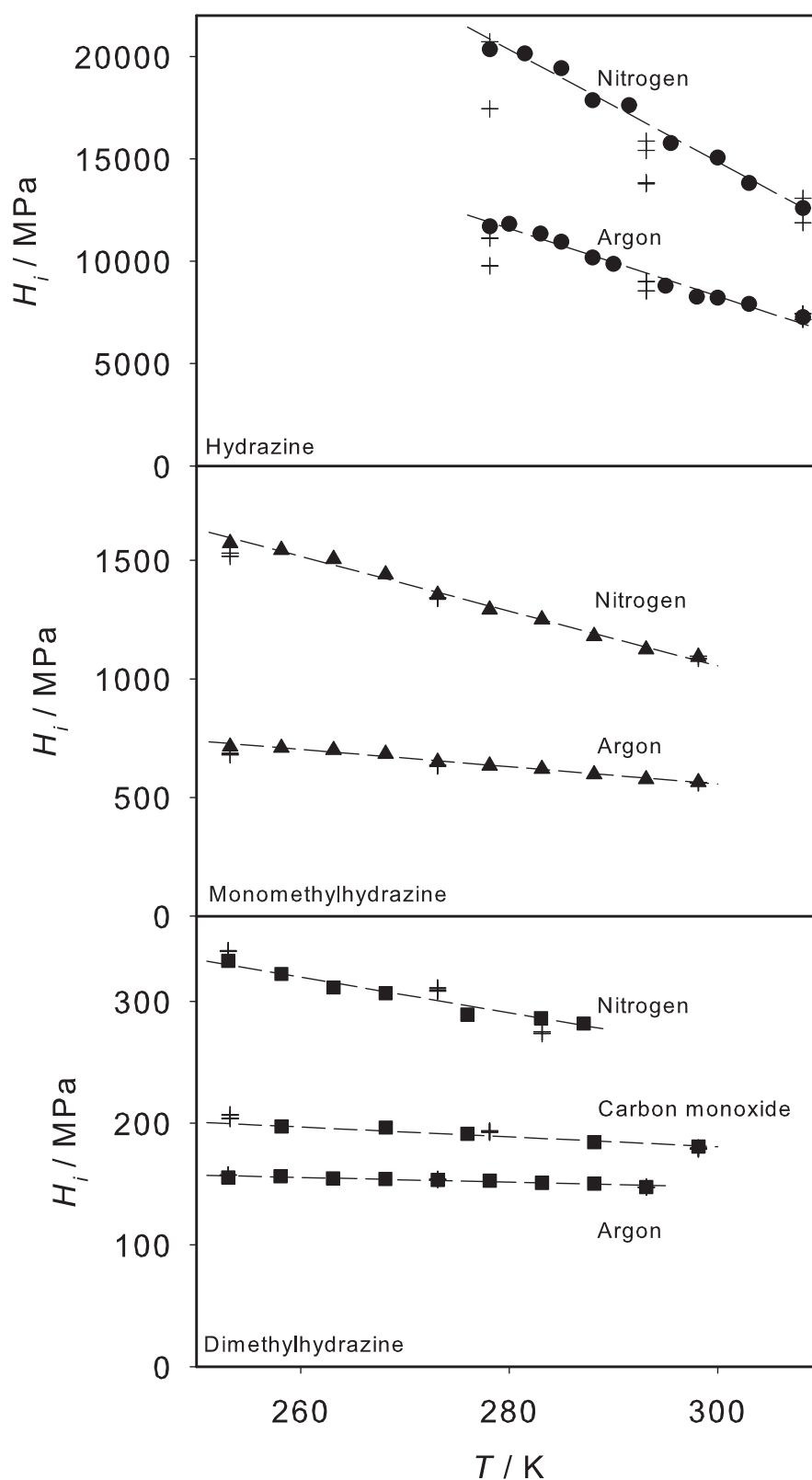
Fig. 14. Henry's law constant of gases in liquid Hydrazine, Monomethylhydrazine and Dimethylhydrazine: (+) experimental data by Chang et al. [62,63]; (●) present simulation data for Argon and Nitrogen in Hydrazine with $\xi=1.02$ (Ar) and $\xi=1.11$ (N$_2$); (▲) present simulation data for Argon and Nitrogen in Monomethylhydrazine with $\xi=0.933$ (Ar) and $\xi=0.976$ (N$_2$); (■) present simulation data for Argon, Nitrogen and Carbon Monoxide in Dimethylhydrazine with $\xi=0.945$ (Ar), $\xi=0.955$ (N$_2$) and $\xi=1.005$ (CO); (- - -) straight lines. The statistical uncertainties of the present data are within symbol size.